5-2015

Mass Table Calculations with Nuclear Density Functional Theory

Noah Watson Birge
University of Tennessee - Knoxville, nbirge@vols.utk.edu

To the Graduate Council:

I am submitting herewith a thesis written by Noah Watson Birge entitled "Mass Table Calculations with Nuclear Density Functional Theory." I have examined the final electronic copy of this thesis for form and content and recommend that it be accepted in partial fulfillment of the requirements for the degree of Master of Science, with a major in Physics.

Witold Nazarewicz, Major Professor

We have read this thesis and recommend its acceptance:

Kate Grzywacz Jones, Thomas Papenbrock

Accepted for the Council:
Dixie L. Thompson

Vice Provost and Dean of the Graduate School

(Original signatures are on file with official student records.)

5-2015

Mass Table Calculations with Nuclear Density Functional Theory

Noah Watson Birge
University of Tennessee - Knoxville, nbirge@vols.utk.edu

To the Graduate Council:

I am submitting herewith a thesis written by Noah Watson Birge entitled "Mass Table Calculations with Nuclear Density Functional Theory." I have examined the final electronic copy of this thesis for form and content and recommend that it be accepted in partial fulfillment of the requirements for the degree of Master of Science, with a major in Physics.

Witold Nazarewicz, Major Professor

We have read this thesis and recommend its acceptance:

Kate Grzywacz Jones, Thomas Papenbrock

Accepted for the Council:
Carolyn R. Hodges

Vice Provost and Dean of the Graduate School

(Original signatures are on file with official student records.)

Mass Table Calculations with Nuclear Density Functional Theory

A Thesis Presented for the

Master of Science

Degree

The University of Tennessee, Knoxville

Noah Watson Birge

May 2015

To my beloved wife Sarah, without whom I would be adrift...

Acknowledgements

I would like to thank Dr. Witek Nazarewicz for welcoming me into his group as an undergraduate and then supporting me through my graduate career. His guidance and instruction have been integral in my development as both a student and a scientist.

I would like to thank Erik Olsen for his encouragement, help, and advice. Without his aid, my time in graduate school and with the research group would not have gone nearly as smoothly. I would particularly like to thank him for his prodigious and prudent editing of my thesis.

I would like to thank my committee members Dr. Thomas Papenbrock and Dr. Kate Jones for their time and comments in editing my Thesis. I am also grateful for their patience and flexibility in the process of scheduling and performing my thesis defense.

I would like to thank Brad Gardner. Without his time and help, much of my data and work would be lost and unrecoverable.

I would finally like to acknowledge Dr. Marianne Breinig. I am very grateful to her for accepting me into The University of Tennessee's Graduate Physics program. It has been a wonderful experience and has brought me very exciting opportunities.

Abstract

To better understand nuclei and the strong nuclear force, it is useful to analyze global nuclear properties and trends across the nuclear chart. To this end, we utilized Nuclear Density Functional Theory with Skyrme Energy Density Functionals in conjunction with high-performance computing to perform large-scale mass table calculations for even-even nuclei. Using the binding energy, pairing gap, root-mean-square radius, and deformation data from these tables we were able to analyze the two-proton and two-neutron drip lines, neutron skin depth, two-proton radioactivity, and the effect of nuclear deformation on mass filters. We used numerous energy density functionals to assess the statistical and systematic errors associated with our calculations.

Table of Contents

List of Figures

List of Attachments

Chapter 1

Introduction

The ultimate goal of nuclear physics is to obtain a fundamental understanding of the nuclear force and its vast technological and societal implications. As new facilities such as the Facility for Rare Isotope Beams (FRIB) come online and begin accessing previously unobserved portions of the nuclear chart [1], nuclear theory can now have its more extreme predictions compared to experimental data and be changed as necessary.

There are three major categories of nuclear models: *ab initio* methods, shell model (Configuration Interaction) approaches, and self-consistent mean-field techniques which employ nuclear Density Functional Theory (DFT). The range of each of these methods is shown in Figure 1.1 [2]. *Ab initio* methods and Configuration Interaction approaches are limited to light- and medium-mass nuclei due to the large configuration space they require for heavier systems [3]. At present, nuclear DFT is the tool of choice when dealing with nuclei all over the nuclear chart [4].

Nuclear DFT is constructed upon mean-field theory, where individual protons and neutrons move independently within an average potential produced by all of the nucleons present. Since nuclear DFT can be independently applied to a specific nucleus, the theory can be exported across the nuclear landscape with a fairly high level of accuracy [5]. Therefore, utilizing nuclear DFT provides a means by

which to calculate nuclear binding energies, neutron and proton radii, and many other properties for nuclei across the entire nuclear landscape ($2 \leq Z \leq 120$ and $2 \leq N \leq 300$) [4, 6–9]. By employing DFT, one can apply an embarrassingly-parallel computational framework to produce calculations across the nuclear landscape and analyze global nuclear properties which can then be compared to those of the ever expanding experimental frontier.

This work focuses on the analysis of global nuclear properties amongst different Skyrme energy density functionals (EDFs) and the comparison of some properties to experimental data. The properties which we considered were binding energies, proton and neutron pairing gaps, nuclear radii, and shape deformation. These properties were obtained directly from large-scale mass table calculations. Using these data, we investigated the two-proton and two-neutron drip lines, uncertainties in neutron-skin values, and the process of two-proton decay. Additionally, in an effort to better understand the interactions which govern some of our calculations, we also analyzed the effect of octupole deformation on various mass filters.

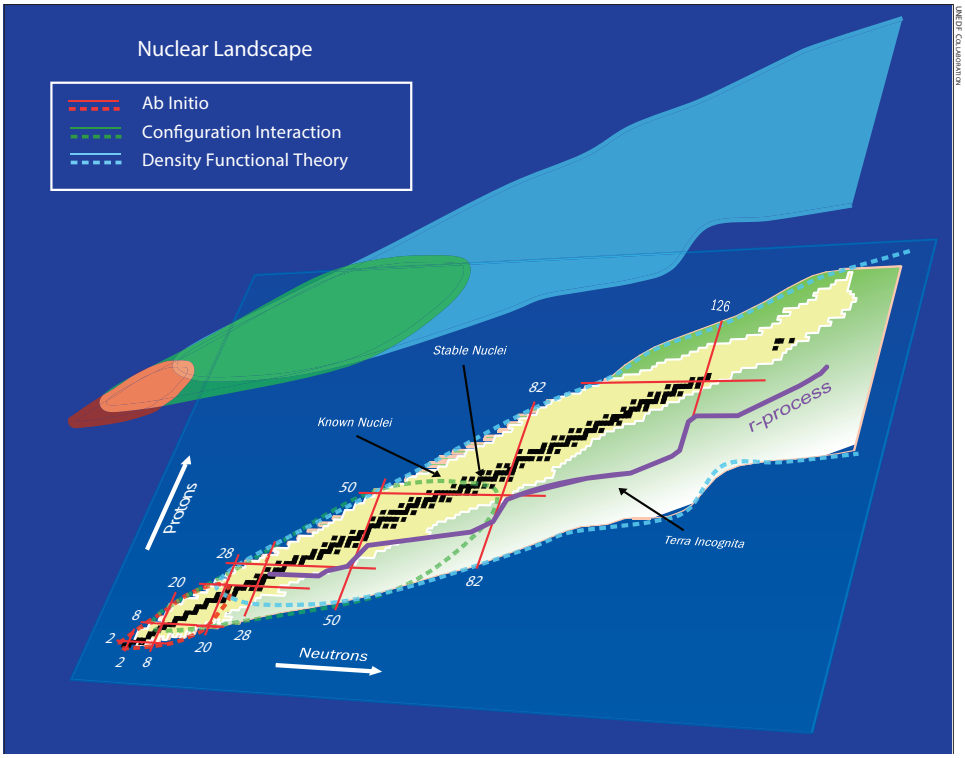

Figure 1.1: The reach of current nuclear models [2]

Chapter 2

Microscopic Nuclear Mass Table with High-Performance Computing

This chapter is a summary of the following published work:

- J. Erler, N. Birge, M. Kortelainen, W. Nazarewicz, E. Olsen, A. Perhac, and M. Stoitsov, "Microscopic nuclear mass table with high-performance computing", *JPCS*, **402**, 012030 (2012)

The original work can be found in **Appendix A**.

2.1 Overview

As was mentioned in Chapter 1, nuclear theory essentially consists of three different approaches. *Ab initio* and configuration interaction models are generally only applicable to light- and medium-mass nuclei, since the configuration space required for either approach very rapidly increases with the number of nucleons present. Nuclear DFT is a mean-field theory, hence all of the nucleons in a system are subjected to an *average* nuclear potential. This construction of the nuclear interaction effectively reduces the size of the required configuration space and allows for ground-state properties to be calculated from very light to very heavy and exotic nuclei.

We take the Skyrme-HFB method to approach the self-consistent Hartree-Fock-Bogoliubov (HFB) problem [3]. This approach is based on local nuclear densities and currents [3, 10, 11]. The self-consistent HFB equations are solved numerically by the computational code HFBTHO [12]. Due to the independent nature of the solutions, the code can be implemented across the nuclear chart (one processor per nucleus) in an embarrassingly parallel scheme. We consider the following six Skyrme EDFs: SkM* [13], SkP [10], SLy4 [14], SV-min [15], UNEDF0 [8], and UNEDF1 [9]. For each of these six parameterizations, we calculate ground-state properties for even-even nuclei with $N \leq 300$ and $Z \leq 120$ on the JAGUAR XT5 supercomputer.

2.2 My Contributions

- Performed the large-scale mass table calculations on the JAGUAR and KRAKEN supercomputers for the following Skyrme EDF parameterizations: SkM*, SLy4, SkP, UNEDF0, UNEDF1, and SV-min.
- Aided in the creation of figure 3.
- Proofreading and editing of the accepted paper.

Chapter 3

The Limits of the Nuclear Landscape

This chapter is a summary of the following published work:

- J. Erler, N. Birge, M. Kortelainen, W. Nazarewicz, E. Olsen, A. Perhac, and M. Stoitsov, "The limits of the nuclear landscape", *Nature* **486**, 509 (2012).

The original work can be found in **Appendix B**.

3.1 Overview

With the aforementioned nuclear mass tables, we can now make global predictions with respect to ground-state nuclear properties and also gauge the statistical and systematic errors of our calculations. With this information, we can make a prediction on the maximum number of nuclei stable to nucleon emission.

The proton or neutron separation energy is defined as the amount of energy needed to remove said nucleon from a specific nucleus. The one-proton and one-neutron separation energies are defined as

$$S_p(Z,N) = B(Z-1,N) - B(Z,N) \tag{3.1}$$

$$S_n(Z,N) = B(Z,N-1) - B(Z,N) \tag{3.2}$$

where $B(Z,N)$ denotes the binding energy of a nucleus with Z protons and N neutrons. Our binding energies are defined to be positive, thus when separation energy is less than zero, the nucleus in unstable with respect to nucleon emission. Therefore, the stable nuclear landscape consists of all nucleons with positive proton and neutron separation energies. The drip lines, which are composed of the last nuclei stable, mark these boundaries of the nuclear chart.

Nuclear pairing generally tends to stabilize even-even species with respect to their odd-mass or odd-odd neighbors [16]. Due to this stabilization, the one-nucleon drip lines are reached earlier in the nuclear landscape than the two-nucleon drip lines, which is discussed in greater detail in **Appendix B**. Since the focus of this work is to predict the maximum number of bound nuclei, we focus on two-proton and two-neutron separation energies defined as follows

$$S_{2p}(Z,N) = B(Z-2,N) - B(Z,N) \tag{3.3}$$

$$S_{2p}(Z,N) = B(Z,N-2) - B(Z,N) \tag{3.4}$$

For each of the six EDF parameterizations previously mentioned, the nuclear drip lines were determined. The systematic uncertainty was then calculated for both the two-proton and two-neutron drip lines, and a summary of these calculations can be seen in Figure 1 of **Appendix B**. Although the uncertainty in the position of the two-neutron drip line grows with the distance from the valley of stability, the consistency between EDFs was much greater than initially expected. This consistency is exemplified in regions near magic nuclear numbers (2, 8, 20, 28, 50,82,126,184).

We also analyzed separation energies along various isotopic chains to analyze the statistical uncertainties. We compared these results to the predictions of the FRDM [17] and HFB-21 [18] models, along with experimental data. Our results for the erbium isotopic chain can be seen in Figure 2 of **Appendix B**. As N increases along the isotopic chain, the statistical uncertainty steadily increases, as expected. However away from the drip lines, we see good consistency not only between the considered EDFs, but also with experimental data and predictions made by the Finite Range Droplet Model (FRDM) [17] and the HFB-21 [18] interaction.

Having determined the predicted drip lines for each functional, we then determined the number of stable nuclei predicted for each parameterization, including the odd-mass and odd-odd nuclei. We predict that $6,900 \pm 500_{syst}$ nuclei are bound with respect to nucleon emission [16].

3.2 My Contributions

- Filtered the data to reflect the nuclear chart of only particle-bound nuclei.
- Aided in the creation of the following figures:
    1. Figure 1
        - Performed drip line analysis of the six mass tables using S_{2n} and S_{2p} values along with λ_n and λ_p. Once the drip line was established for each parametrization, an average drip line was calculated, along with its uncertainty.
    2. Figure 2
        - For the six functionals and the FRDM and HFB-21 models, similar plots were created along various isotopic chains, including erbium.
    3. Supplementary Figures 2-4
- Proofreading and editing of the letter and the supplementary paper.

Chapter 4

Neutron-skin Uncertainties of Skyrme Energy Density Functionals

This chapter is a summary of the following published work:

- M. Kortelainen, J. Erler, W. Nazarewicz, N. Birge, Y. Gao, and E. Olsen, "Neutron-skin uncertainties of Skyrme energy density functionals", *Phys. Rev. C*, **88**, 031305(R) (2013)

The original work can be found in **Appendix C**.

4.1 Overview

An invaluable aspect of theoretical calculations of global nuclear properties is that these predictions can be quickly compared to experimental data, which allows nuclear theory to pin down key parameters. To this effect, we consider nuclear radii. More specifically, we consider neutron skin thickness defined as the difference of neutron

and proton point root-mean-square radii:

$$r_{skin} = < r_n^2 >^{1/2} - < r_p^2 >^{1/2} \tag{4.1}$$

for the six functionals above. Experiments such as The Lead Radius Experiment (PREX) [19], the follow up experiment PREX-II [20], and The Calcium Radius Experiment (CREX) [21] could provide useful constraints on nuclear DFT parameters, provided the uncertainty in the measurements is smaller than the uncertainty in the calculations. Thus we perform a global study of the systematic error, and provide a statistical analysis of the theoretical error for calcium and lead nuclei, along with a few isotopic chains.

A summary of the systematic uncertainty analysis of r_{skin} can be seen in Figure 1 of **Appendix C**. As expected, the average neutron skin thickness and its systematic uncertainty both increase with N [22, 23]. As was seen along the drip lines Chapter 3, the systematic uncertainty in r_{skin} is also fairly small, not exceeding 0.05 fm for very neutron-rich systems. Once again, these EDFs yield very consistent findings, despite having different optimization strategies.

We next considered the statistical uncertainty in r_{skin} along several isotopic chains for the UNEDF0 and SV-min EDFs. The isotopes considered were calcium, zirconium, erbium, and $Z = 120$, the results of which can be seen in Figure 2 of **Appendix C**. The statistical errors in ^{48}Ca and ^{208}Pb were also considered and compared to both the accuracy of PREX and the predicted accuracies of PREX-II and CREX. The following table (taken directly from the work) can be seen below.

Having found that the statistical uncertainty is less than the accuracy of the PREX and PREX-II experiments, they are unlikely to provide any useful constraints on isovector coupling constants of the theory. However, the predicted 0.02 fm accuracy of CREX [21] should be able to supply useful constraints.

Table 4.1: Theoretical uncertainties on r_{skin} in ^{208}Pb and ^{48}Ca (in fm). (Taken directly from the table in **Appendix C**.) Shown are statistical errors of UNEDF0 and SV-min, systematic error Δr^{syst}_{skin}, the model-averaged deviation of Ref. [24], and errors of PREX [19] and planned PREX-II [20] and CREX [21] experiments.

Nucleus	Δr^{stat}_{skin}		Δr^{syst}_{skin}	Ref. [24]	Experiment
	UNEDF0	SV-min			
^{208}Pb	0.058	0.037	0.013	0.022	0.18 [19], 0.06[20]
^{48}Ca	0.035	0.026	0.019	0.018	0.02 [21]

4.2 My Contributions

- Using the aforementioned HFBTHO mass table data, calculated r^{av}_{skin} and Δr^{syst}_{skin}.
- Aided in the development and production of Figure 1 (a) and (b).
- Proofreading and editing of the accepted paper.

Chapter 5

The Landscape of Two-Proton Radioactivity

This chapter is a summary of the following published works:

- E. Olsen, M. Pfützner, N. Birge, M. Brown, W. Nazarewicz, and A. Perhac, "Landscape of Two-Proton Radioactivity", *Phys. Rev. Lett.*, **110**, 222501 (2013)
- E. Olsen, M. Pfützner, N. Birge, M. Brown, W. Nazarewicz, and A. Perhac, "Erratum: Landscape of Two-Proton Radioactivity", *Phys. Rev. Lett.*, **111**, 139903 (2013)

The original works can be found in **Appendix D**, and **Appendix D: Erratum**.

5.1 Overview

By analyzing ground-state global nuclear properties calculated for the six different EDFs, one can estimate various nuclear properties, such as decay lifetimes. With these lifetimes, one can perform a systematic check of the theory and the corresponding predictions, which can then be compared to experimental data. One such property

of particular interest is two-proton ($2p$) radioactivity, where two protons are ejected from an unbound nucleus (nuclei beyond the proton drip line). Motivated by the experimental discovery of $2p$ emission in ^{45}Fe [25, 26], ^{19}Mg [27], ^{48}Ni [28], and ^{54}Zn [29] we perform a global analysis of this decay path, as it has not been performed above strontium [30–34]. Thus this work aims to not only illuminate a global region of $2p$ radioactivity, but also to determine the best candidates to experimentally observe this process.

Within our global survey of $2p$ radioactivity, we attempt to maximize the number of possible emitters. To this end, we consider two types of $2p$ decay: sequential and simultaneous. Sequential decay occurs when one proton is emitted from the nucleus followed by emission of a second proton some (relatively short) time later. Simultaneous decay is when both protons leave the nucleus at the same time as a correlated pair. To determine nuclei that could be potential candidates, we impose the energetic criteria seen in **Appendix D: Erratum**. These two criteria function as less stringent energetic requirements that allow for the maximum number of candidates to be determined.

To determine $2p$ half-lives, we considered two different decay models, the diproton model and the direct decay model. The former is outlined in refs. [30, 31, 35], and the latter is outlined in refs. [35–37]. With these half-lives calculated, we then imposed the lifetime criteria seen in equations (2) and (3) of **Appendix D**. The lower bound of Eq. (2) is imposed since time scales of this magnitude mark the limit of sensitivity for typical in-flight projectile fragmentation techniques [37]. The upper bound ensures that the nucleus is not dominated by β decay. The criterion of Eq. (3) removes any fast α emitters from our pool of candidates. To determine potential nuclei with α decay and $2p$ decay competition, we also explore candidates which fulfill $0.1T_{2p} \leq T_{\alpha} \leq 10T_{2p}$. Our results our summarized in Figs. (1) and (2) of **Appendix D: Erratum**.

We find that sequential and simultaneous decay are predicted to occur up to Te, after which, only sequential decay is predicted to exist. After Pb, we find that α

decay is the only decay path and $2p$ decay is very unlikely to be observed. Finally, we predict that the best candidates for experimental observation of $2p$ decay are ^{57}Ge, ^{62,63}Se, ^{66}Kr, and ^{103}Te. These nuclei are located only a few neutrons away from currently known isotopes and are predicted by both decay models and multiple EDFs. The best candidates predicted to exhibit α decay and $2p$ decay competition are ^{103}Te and ^{145}Hf.

5.2 My Contributions

- Utilized the above mass table calculation data to calculate various properties such as T_{2p} and Q_{2p}.
- Aided in the approximation of T_{2p} by running a WKB approximation code with the above data as input.
  - The above data was then compared to experimentally known $2p$ emitter lifetimes.
- Applied various criteria for nuclei to be admitted to the $2p$ decay landscape.
- Calculated *model multiplicity* to determine the average $2p$ trajectory.
- Aided in the production of Figure 1 via the above data and data filtering.
- Aided in the production of Figure 2 in a similar fashion.
- Proofreading and editing of the letter and erratum.

Chapter 6

Octupole Deformation Effects on Mass Filters

6.1 Introduction

Differences of global nuclear properties can provide insight into the interactions that govern the nucleus. Here, we focus on differences of binding energy and compare said differences in regions of stronger octupole deformation, namely the even-even actinides and lanthanides. The mass filters considered were: two neutron separation energy S_{2n}, two proton separation energy S_{2p}, and the double-difference indicator δV_{pn}. From these investigations, we can perform future work on exploring this effect on these mass filters and gain some deeper understanding of the interactions which we have incorporated into our models.

All of the above work has been accomplished with the code HFBTHO, which does not presently include a reflection asymmetric degree of freedom. With the development of the code AxialHFB, we can now explore reflection-asymmetric deformations in nuclear ground states across the nuclear landscape for four different functionals: UNEDF0, UNEDF1, UNEDF2 [38], and SV-min (see Fig. 6.1). With these calculations at hand, we would like to investigate the effect of β_3 deformation

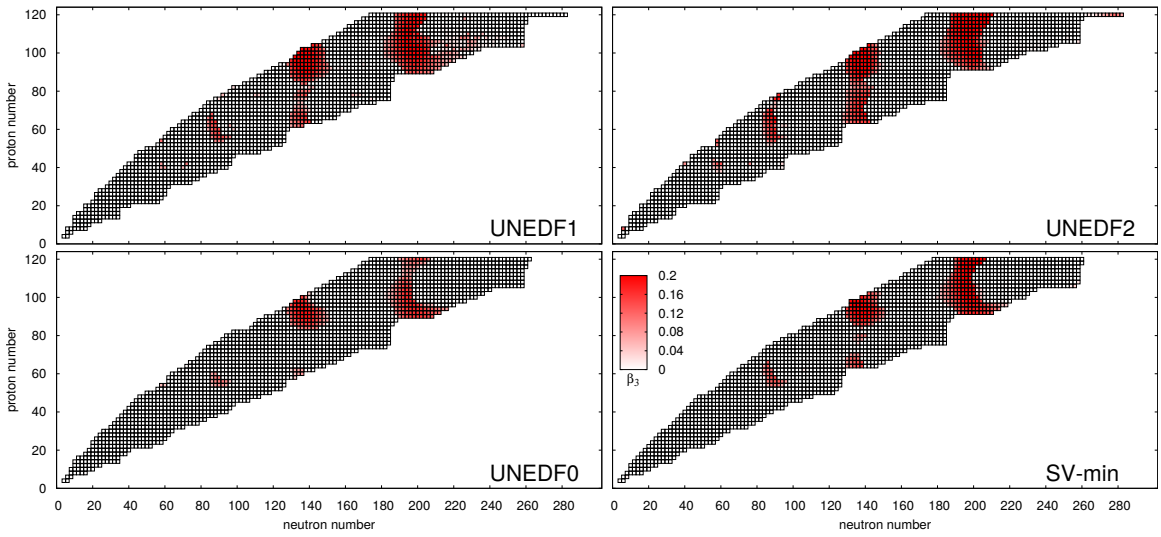

Figure 6.1: The landscape of ground-state β_3 deformation. The above are the calculated ground-state β_3 deformations for even-even nuclei for $Z \leq 120$ and $N \leq 300$. Note that since one of the mass-filters in question is δV_{pn}, only the stable nuclei with well defined δV_{pn} are plotted.

on the two-proton and two-neutron separation energies, and δV_{pn} mass filters. As discussed in Chapter 3, separation energies are the primary factor in determining the stability of nuclei. Hence, with AxialHFB available for four different functional parameterizations, we would like to analyze any possible effect of β_3 these mass filters that are vital for shaping the nuclear landscape.

The δV_{pn} mass filter functions as a somewhat different indicator than the aforementioned separation energies for our analysis. As outlined in refs. [39–41],

$$\delta V_{pn} = \frac{1}{4}\{B(Z,N) - B(Z,N-2) - B(Z-2,N) + B(Z-2,N-2)\} \tag{6.1}$$

and represents the following mixed partial derivative [42]:

$$\delta V_{pn}(Z,N) \approx \frac{\partial^2 B}{\partial Z \partial N} \tag{6.2}$$

The proton-neutron interaction clearly performs a vital role in finite nuclear matter, particularly the development of deformation in nuclei [39, 43]. Therefore with

constrained ($\beta_3 = 0$) and unconstrained calculations, we may then probe the proton-neutron interaction of actinides and lanthanides, where octupole deformation becomes much more important [40, 44].

6.2 Analysis

To verify that our constrained calculations produced nearly equivalent β_2 deformations as our unconstrained calculations, we plotted β_2 (and β_3) against neutron number for all of the even-even actinide and lanthanide isotopic chains. We found, as expected, that β_2 values for the constrained calculations followed the general trend of those for the unconstrained calculations closely, with a few very minor discrepancies where β_2 deformation began earlier along the isotopic chains for the unconstrained calculations. Otherwise, the results agree quite well.

We next examined S_{2n} and S_{2p} differences between the two calculations. Away from regions of octupole deformation, the plots lay virtually on top of one another, but we found a functional-independent trend in octupole deformed regions. As β_3 begins to increase from zero, the unconstrained values fall below the constrained values by up to 1 MeV. Then, as β_3 approaches a maximum value along the chain, the unconstrained value of S_{2n} falls below the constrained and gradually the two values converge as β_3 returns to zero. The S_{2p} difference is not as nearly as pronounced. As expected, the main difference occurs in regions of octupole deformation, and the plots are essentially identical for the rest of the isotopic chain. In those regions of $\beta_3 \neq 0$, the unconstrained values of S_{2p} are slightly larger (generally less than 0.5 MeV) than the constrained values S_{2p}. Figures 6.2-6.9 show the S_{2n} and S_{2p} results for thorium and neodymium.

Finally, we compared unconstrained and constrained values of δV_{pn}. Although the differences are larger between the isotopic chains, this is to be expected, as δV_{pn} involves the differences of the binding energies of four different nuclei and the δV_{pn} energy scale is much smaller. As with S_{2n} and S_{2p} we see the largest variation between

the unconstrained and constrained calculations occurs in the region of nonzero β_3. In those regions, we see that the unconstrained δV_{pn} maxima are shifted neutrons up or down the isotopic chain. Although the shift is generally consistent between functional parameterizations, there does not appear to be much of a correlation between Z and the location of the peak (see figures 6.2-6.9).

6.3 Future Work

Having analyzed the results of four different functional paramaterizations, the next step to take will be to obtain large-scale mass table calculations for the following functionals: SkP, SkM*, and SLy4. With said results, a similar analysis to the above will be performed. We will then proceed to compare our calculations to experimental data in order to perform an assessment of our predictions. Finally, in a similar fashion as we did in Chapter 3, an error analysis may be performed for the AxialHFB computational framework.

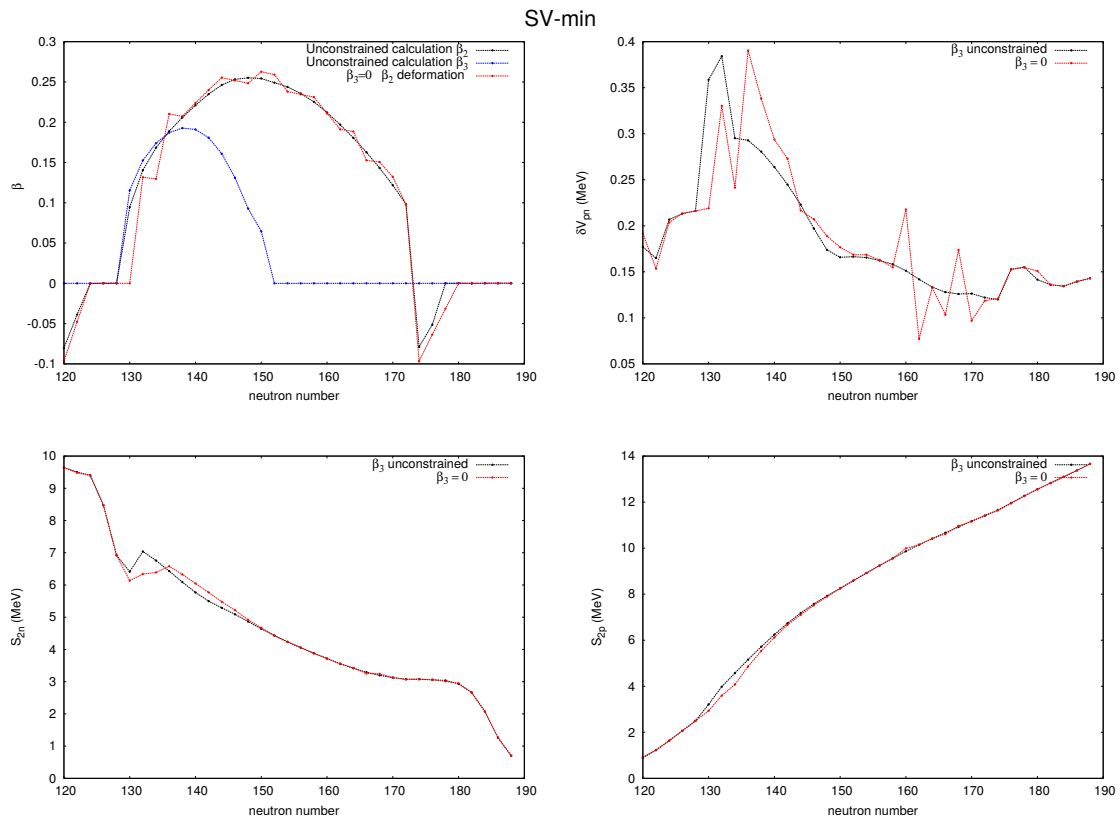

Figure 6.2: β_3 Deformation effect on thorium Mass Filters. Above is the comparison of δV_{pn}, S_{2n}, and S_{2p} for constrained and unconstrained AxialHFB calculations along the thorium isotopic chain for the SV-min functional parameterization.

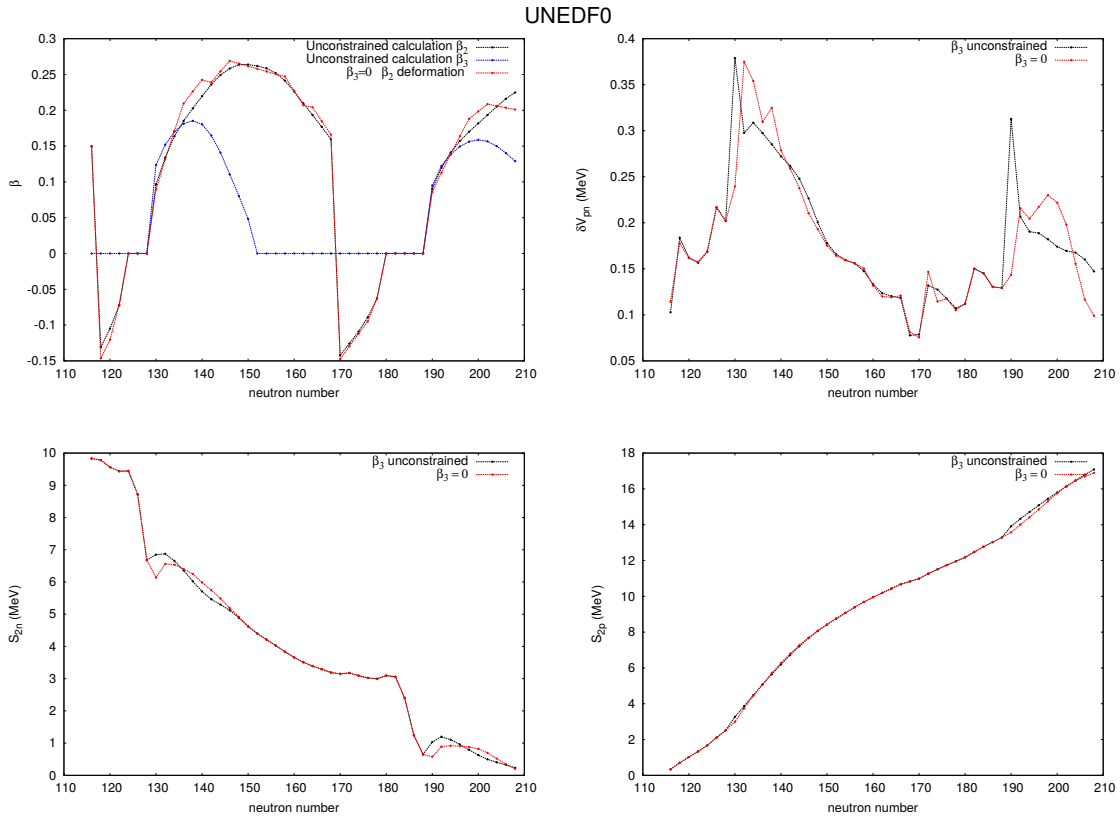

Figure 6.3: Same as Figure 6.2 but for UNEDF0.

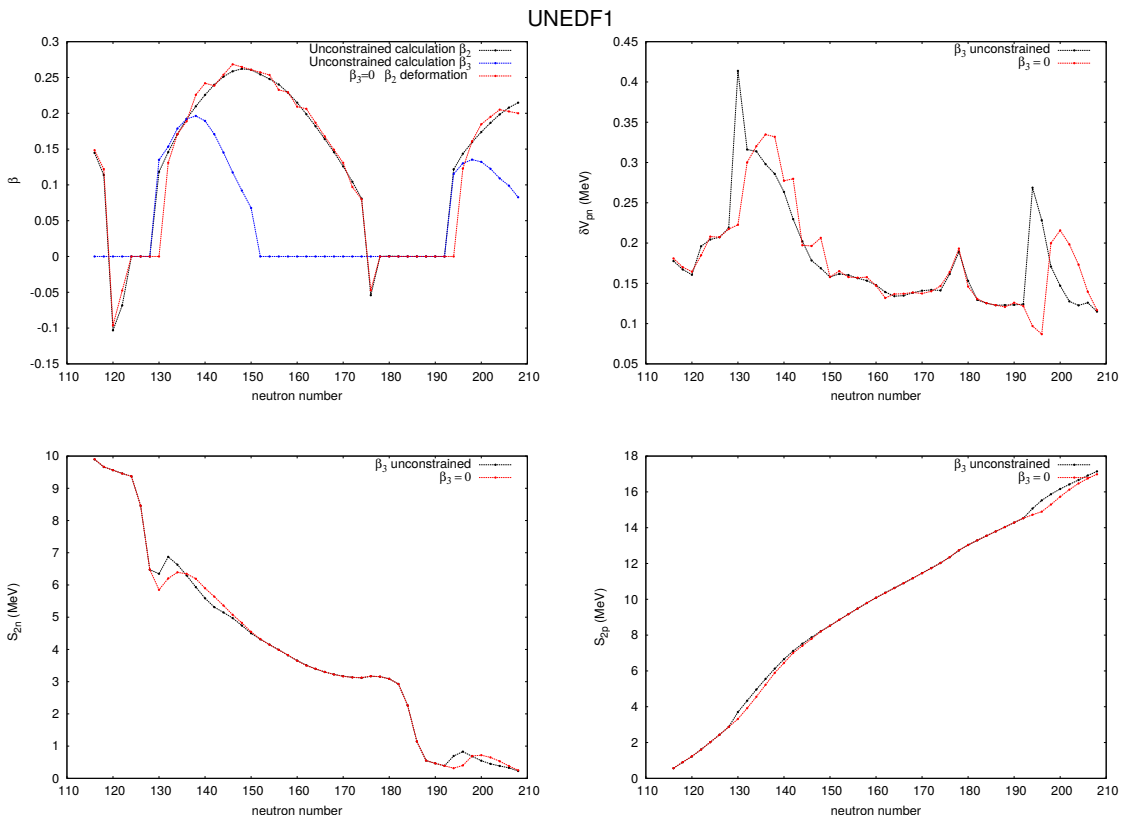

Figure 6.4: Same as Figure 6.2 but for UNEDF1

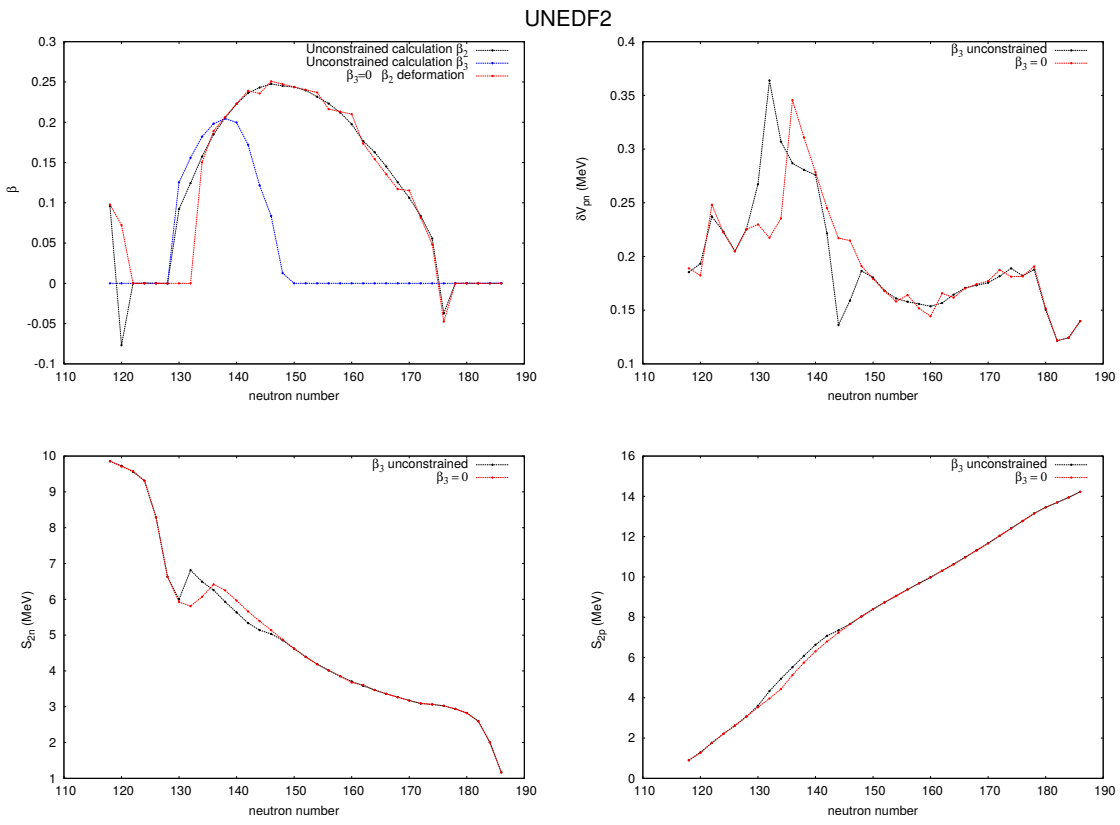

Figure 6.5: Same as Figure 6.2 but for UNEDF2

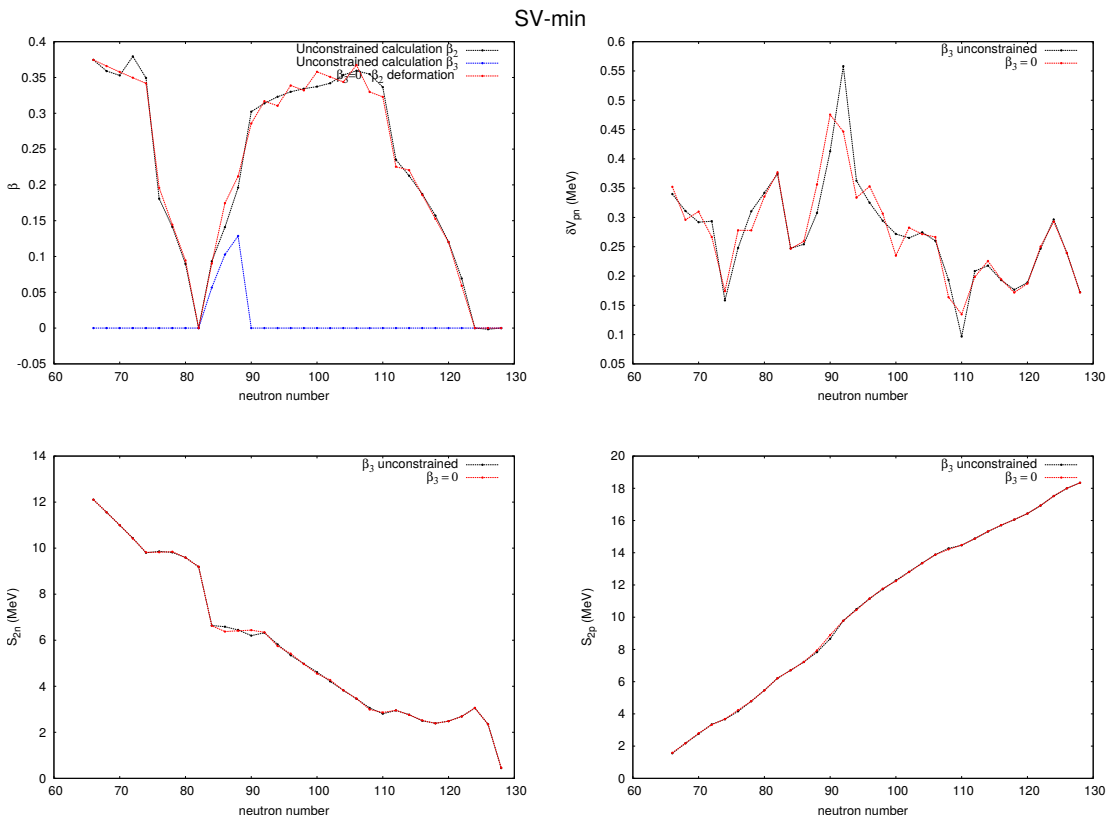

Figure 6.6: β_3 Deformation effect on neodymium mass filters. Above is the comparison of δV_{pn}, S_{2n}, and S_{2p} for constrained and unconstrained AxialHFB calculations along the neodymium isotopic chain for the SV-min functional parameterization.

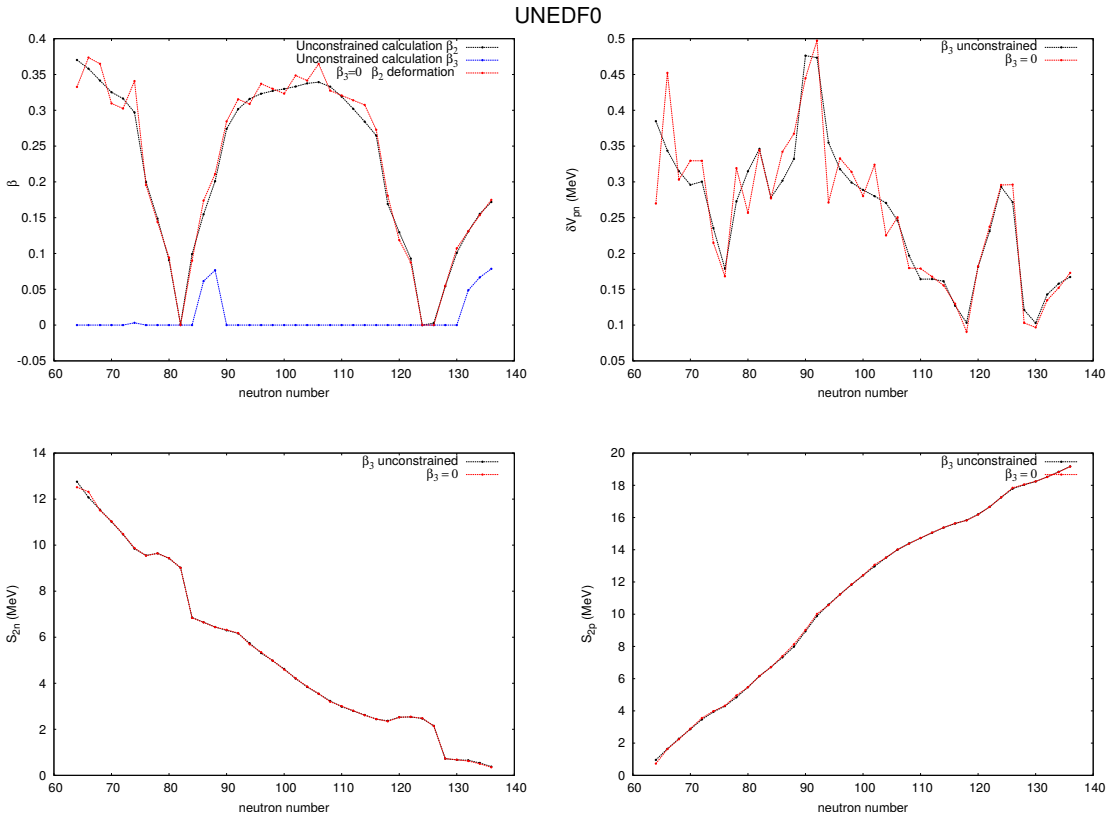

Figure 6.7: Same as Figure 6.6 but for UNEDF0.

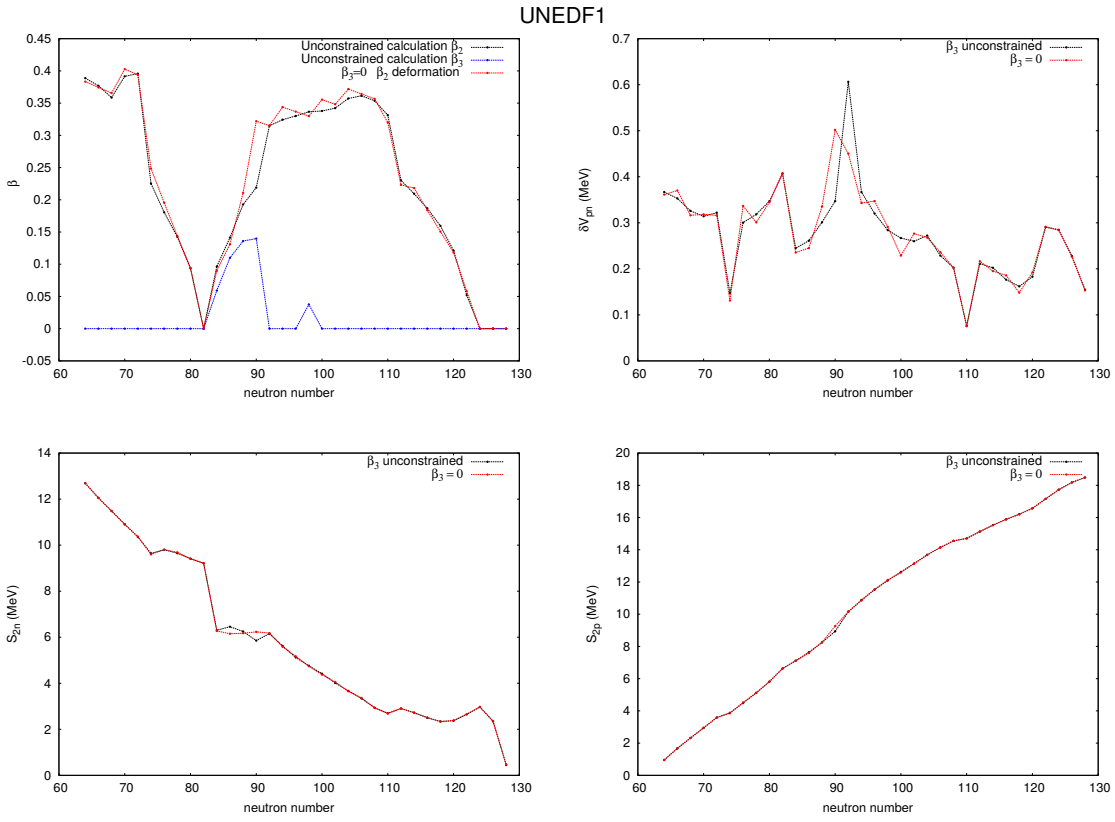

Figure 6.8: Same as Figure 6.6 but for UNEDF1.

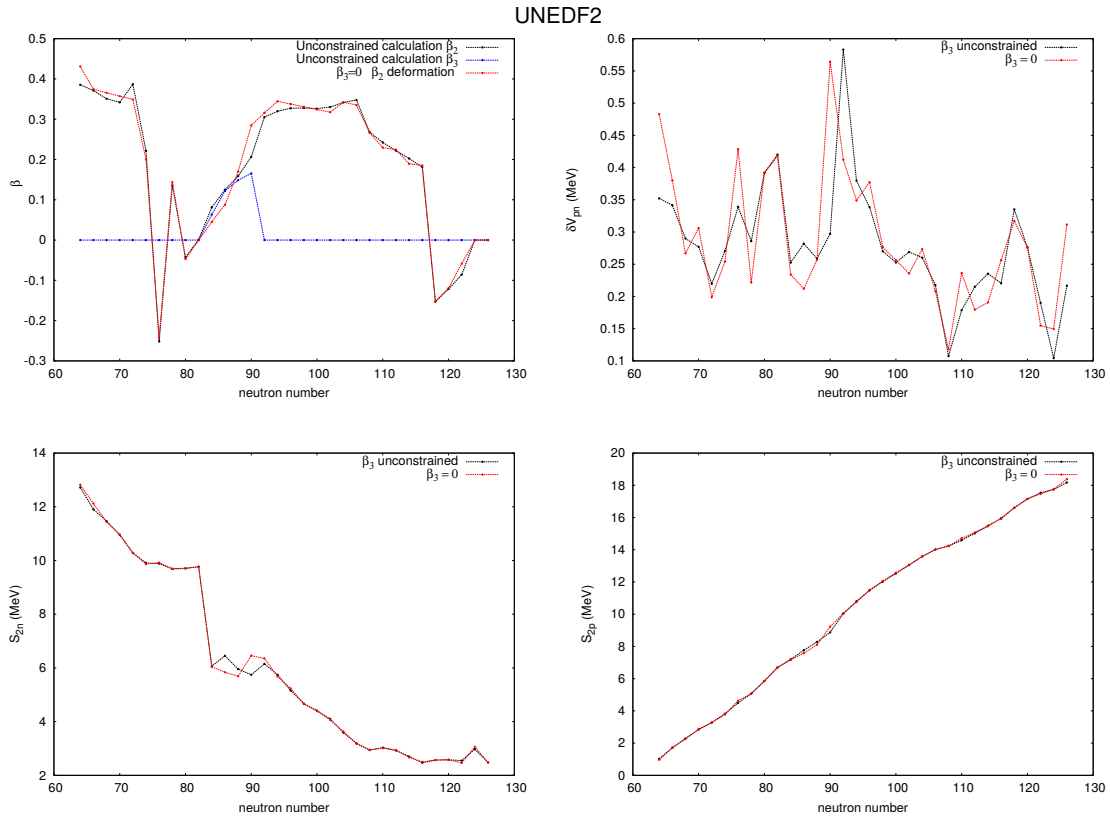

Figure 6.9: Same as Figure 6.6 but for UNEDF2.

6.4 My Contributions

- Performed large-scale AxialHFB mass table calculations on the Darter and Eos ORNL clusters based on the following functional parametrizations: SV-min, UNEDF0, UNEDF1, and UNEDF2.
- Performed δV_{pn}, S_{2n}, and S_{2p} calculations from the output of the above calculations.
- Filtered and analyzed the above mass filter data
- Created deformation, δV_{pn}, S_{2n}, and S_{2p} plots along even-even isotopic chains for the actinides and lanthanides.

Chapter 7

Conclusion

Large-scale computing plays an integral role in modern theoretical nuclear physics. By utilizing the nuclear DFT framework, calculations of ground state nuclear properties can be exported across the entire nuclear landscape. Thus by analyzing and examining global nuclear properties and comparing the results with experimental data, one can quickly gauge the robustness of nuclear DFT and Skyrme EDFs. In this work, we primarily focused on ground-state binding energies, nuclear radii, pairing gaps and energies, and shape deformation data.

7.1 Microscopic Nuclear Mass Table with High-Performance Computing

In Chapter 2 we outlined the computational framework of our calculations from the HFBTHO code. We then discussed how some of the tabulated global nuclear properties can be calculated in a relatively small period of time using nuclear DFT with various Skyrme EDF parameterizations. Finally, we discussed the applicability of these large-scale calculations and their potential in future work.

7.2 The Limits of the Nuclear Landscape

In Chapter 3 we briefly reviewed the current status of the experimental and theoretical nuclear landscape. We then delineated the role of one- and two-nucleon separation energies along with nucleonic chemical potentials in shaping the boundaries of nuclear binding, the proton and neutron drip lines. Based on six different functional parameterizations of our mass-table calculations, we assessed the systematic and statistical error bars involved with our calculations. We also compared our calculations to those predicted by other models and found relatively sound agreement. Thus, having established a fairly consistent nuclear boundary, we predicted the existence of $6,900 \pm 500_{syst}$ nuclei that are bound to nucleon emission with $Z \leq 120$.

7.3 Neutron-skin Uncertainties of Skyrme Energy Density Functionals

In Chapter 4 we examined nuclear radii and their uncertainties across our nuclear mass-table calculations. Since these predictions are vital for neutron star equations-of-state, we estimated our theoretical systematic and statistical uncertainties on neutron skin thickness. We found that our uncertainty in neutron-skin increased with neutron excess and that our statistical errors associated with this property were larger than the systematic error across the landscape. Also, our results show that the upcoming CREX experiment should have the necessary accuracy to reduce statistical error on future neutron-skin calculations.

7.4 The Landscape of Two-Proton Radioactivity

In Chapter 5 we analyzed global two-proton radioactivity based on our nuclear mass-table data. Using one- and two-proton separation energies and pairing gaps, we

calculated $2p$ decay widths and lifetimes. Based on the consistency of our functionals, we predicted strong candidates for experimental observation of $2p$ emission. We also determined systems in which there would be noticeable competition between α-decay and $2p$ emission. We also determined that above lead, $2p$-decay does not exist and α-decay is the dominant decay path.

7.5 Octupole Deformation Effects on Mass Filters

In Chapter 6 we utilized the new computer code AxialHFB to explore the effect of reflection asymmetric shape deformations in nuclei. We examined the mass filters S_{2n}, S_{2p}, and δV_{pn} along lanthanide and actinide isotopic chains for constrained ($\beta_3 = 0$) and unconstrained calculations. There was found to be very little difference in the two calculations with respect to S_{2p}, however for S_{2n}, the energies of the unconstrained calculations were found to be larger than the constrained calculations until maximum β_3 deformation was reached. δV_{pn} maxima along isotopic chains also appeared to be shifted by a few neutrons, depending on the specific isotope. Further work is to be done with the aforementioned functionals to get a better handle on uncertainties associated with our data and finally, the seven mass table calculations will be compared to experimental values.

Bibliography

[1] E. Reich, "Isotope factory accelerates," *Nature*, vol. 477, p. 15, 2011. 1

[2] G. Bertsch, D. J. Dean, and W. Nazarewicz, "Universal Nuclear Energy Density Functional: Computing Atomic Nuclei," *SciDac Review*, vol. 6, pp. 42–51, 2007. 1, 3

[3] M. Bender, P.-H. Heenen, and P.-G. Reinhard, "Self-consistent mean-field models for nuclear structure," *Rev. Mod. Phys.*, vol. 75, pp. 121–180, Jan 2003. 1, 5

[4] M. Stoitsov, J. Dobaczewski, W. Nazarewicz, and P. Borycki, "Large-scale self-consistent nuclear mass calculations," *IJMS*, vol. 251, no. 2-3, pp. 243 – 251, 2006. 1, 2

[5] S. Goriely, N. Chamel, and J. M. Pearson, "Skyrme-Hartree-Fock-Bogoliubov Nuclear Mass Formulas: Crossing the 0.6 MeV Accuracy Threshold with Microscopically Deduced Pairing," *Phys. Rev. Lett.*, vol. 102, p. 152503, Apr 2009. 1

[6] M. V. Stoitsov, J. Dobaczewski, W. Nazarewicz, S. Pittel, and D. J. Dean, "Systematic study of deformed nuclei at the drip lines and beyond," *Phys. Rev. C*, vol. 68, p. 054312, Nov 2003. 2

[7] M. Stoitsov, W. Nazarewicz, and N. Schunck, "Large-scale mass table calculations," *Int. J. Mod. Phys. E*, vol. 18, pp. 816–822, 2009.

[8] M. Kortelainen *et al.*, "Nuclear energy density optimization," *Phys. Rev. C*, vol. 82, p. 024313, Aug 2010. 5

[9] M. Kortelainen *et al.*, "Nuclear energy density optimization: Large deformations," *Phys. Rev. C*, vol. 85, p. 024304, Feb 2012. 2, 5

[10] J. Dobaczewski, H. Flocard, and J. Treiner, "Hartree-Fock-Bogolyubov description of nuclei near the neutron-drip line," *Nucl. Phys. A*, vol. 422, pp. 103–139, 1984. 5

[11] E. Perlińska, S. G. Rohoziński, J. Dobaczewski, and W. Nazarewicz, "Local density approximation for proton-neutron pairing correlations: Formalism," *Phys. Rev. C*, vol. 69, p. 014316, Jan 2004. 5

[12] M. Stoitsov, J. Dobaczewski, W. Nazarewicz, and P. Ring, "Axially deformed solution of the Skyrme-Hartree-Fock-Bogolyubov equations using the transformed harmonic oscillator basis. The program HFBTHO (v1.66p) ," *Comp. Phys. Comm.*, vol. 167, no. 1, pp. 43 – 63, 2005. 5

[13] J. Bartel, P. Quentin, M. Brack, C. Guet, and H.-B. Håkansson, "Towards a better parametrisation of Skyrme-like effective forces: A critical study of the SkM force ," *Nucl. Phys. A*, vol. 386, no. 1, pp. 79 – 100, 1982. 5

[14] E. Chabanat *et al.*, "Erratum," *Nucl. Phys. A*, vol. 643, no. 4, pp. 441 –, 1998. 5

[15] P. Klüpfel, P.-G. Reinhard, T. J. Bürvenich, and J. A. Maruhn, "Variations on a theme by Skyrme: A systematic study of adjustments of model parameters," *Phys. Rev. C*, vol. 79, p. 034310, Mar 2009. 5

[16] J. Erler, N. Birge, M. Kortelainen, W. Nazarewicz, E. Olsen, A. M. Perhac, and M. Stoitsov, "The limits of the nuclear landscape," *Nature*, vol. 486, pp. 509–512, June 2012. 7, 8

[17] P. Möller, J. Nix, W. Myers, and W. Swiatecki, "Nuclear ground-state masses and deformations," *Atomic Data and Nuclear Data Tables*, vol. 59, no. 2, pp. 185 – 381, 1995. 8

[18] S. Goriely, N. Chamel, and J. M. Pearson, "Further explorations of Skyrme-Hartree-Fock-Bogoliubov mass formulas. XII. Stiffness and stability of neutron-star matter," *Phys. Rev. C*, vol. 82, p. 035804, Sep 2010. 8

[19] S. Abrahamyan *et al.*, "Measurement of the Neutron Radius of ^{208}Pb through Parity Violation in Electron Scattering," *Phys. Rev. Lett.*, vol. 108, p. 112502, Mar 2012. 10, 11

[20] "PREX-II Proposal to Jefferson Lab http://hallaweb.jlab.org/parity/prex/prexII.pdf." 10, 11

[21] "CREX Proposal to Jefferson Lab http://hallaweb.jlab.org/parity/prex/c-rex2013_v7.pdf." 10, 11

[22] S. Mizutori, J. Dobaczewski, G. A. Lalazissis, W. Nazarewicz, and P.-G. Reinhard, "Nuclear skins and halos in the mean-field theory," *Phys. Rev. C*, vol. 61, p. 044326, Mar 2000. 10

[23] J. Dobaczewski, W. Nazarewicz, and T. Werner, "Neutron radii and skins in the Hartree-Fock-Bogoliubov calculations," *Z. Phys. A*, vol. 354, no. 1, pp. 27–35, 1996. 10

[24] J. Piekarewicz, B. K. Agrawal, G. Colò, W. Nazarewicz, N. Paar, P.-G. Reinhard, X. Roca-Maza, and D. Vretenar, "Electric dipole polarizability and the neutron skin," *Phys. Rev. C*, vol. 85, p. 041302, Apr 2012. 11

[25] M. Pfützner *et al.*, "First evidence for the two-proton decay of ^{45}Fe," *Eur. Phys. J. A*, vol. 14, no. 3, pp. 279–285, 2002. 13

[26] J. Giovinazzo *et al.*, "Two-Proton Radioactivity of ^{45}Fe," *Phys. Rev. Lett.*, vol. 89, p. 102501, Aug 2002. 13

[27] I. Mukha *et al.*, "Proton-proton correlations observed in two-proton decay of ^{19}Mg and ^{16}Ne," *Phys. Rev. C*, vol. 77, p. 061303, Jun 2008. 13

[28] M. Pomorski *et al.*, "First observation of two-proton radioactivity in ^{48}Ni," *Phys. Rev. C*, vol. 83, p. 061303, Jun 2011. 13

[29] B. Blank *et al.*, "First Observation of ^{54}Zn and its Decay by Two-Proton Emission," *Phys. Rev. Lett.*, vol. 94, p. 232501, Jun 2005. 13

[30] B. A. Brown, "Diproton decay of nuclei on the proton drip line," *Phys. Rev. C*, vol. 43, pp. R1513–R1517, Apr 1991. 13

[31] W. Nazarewicz *et al.*, "Structure of proton drip-line nuclei around doubly magic ^{48}Ni," *Phys. Rev. C*, vol. 53, pp. 740–751, Feb 1996. 13

[32] B. J. Cole, "Stability of proton-rich nuclei in the upper *sd* shell and lower *pf* shell," *Phys. Rev. C*, vol. 54, pp. 1240–1248, Sep 1996.

[33] W. E. Ormand, "Properties of proton drip-line nuclei at the *sd*-*fp*-shell interface," *Phys. Rev. C*, vol. 53, pp. 214–221, Jan 1996.

[34] B. A. Brown, R. R. C. Clement, H. Schatz, A. Volya, and W. A. Richter, "Proton drip-line calculations and the rp process," *Phys. Rev. C*, vol. 65, p. 045802, Mar 2002. 13

[35] E. Olsen, M. Pfützner, N. Birge, M. Brown, W. Nazarewicz, and A. Perhac, "Landscape of Two-Proton Radioactivity," *Phys. Rev. Lett.*, vol. 110, p. 222501, May 2013. 13

[36] L. V. Grigorenko and M. V. Zhukov, "Two-proton radioactivity and three-body decay. II. Exploratory studies of lifetimes and correlations," *Phys. Rev. C*, vol. 68, p. 054005, Nov 2003.

[37] M. Pfützner, "Particle radioactivity of exotic nuclei," *Phys. Scripta*, vol. 2013, no. T152, p. 014014, 2013. 13

[38] M. Kortelainen *et al.*, "Nuclear energy density optimization: Shell structure," *Phys. Rev. C*, vol. 89, p. 054314, May 2014. 15

[39] R. Cakirli, D. Brenner, R. Casten, and E. Millman, "Proton-Neutron Interactions and the New Atomic Masses," *Phys. Rev. Lett.*, vol. 94, p. 092501, March 2005. 16

[40] M. Stoitsov, R. Cakirli, R. Casten, W. Nazarewicz, and W. Statula, "Empirical Proton-Neutron Interactions and Nuclear Density Functional Theory: Global, Regional, and Local Comparisons," *Phys. Rev. Lett.*, vol. 98, p. 132502, March 2007. 17

[41] J.-Y. Zhang, R. Casten, and D. Brenner, "Empirical proton-neutron interaction energies. Linearity and saturation phenomena ," *Phys. Lett. B* , vol. 227, no. 1, pp. 1 – 5, 1989. 16

[42] W. Satuĺa, D. Dean, J. Gary, S. Mizutori, and W. Nazarewicz, "On the origin of the Wigner energy ," *Physics Letters B* , vol. 407, no. 2, pp. 103 – 109, 1997. 16

[43] I. Talmi, "Effective Interactions and Coupling Schemes in Nuclei," *Rev. Mod. Phys.*, vol. 34, pp. 704–722, Oct 1962. 16

[44] P. A. Butler and W. Nazarewicz, "Intrinsic reflection asymmetry in atomic nuclei," *Rev. Mod. Phys.*, vol. 68, pp. 349–421, Apr 1996. 17

Appendix

Appendix A

Microscopic nuclear mass table with high-performance computing

This information was uploaded as an attachment (see Microscopic-nuclear.pdf).

Appendix B

The limits of the nuclear landscape

This information was uploaded as an attachment (see Limits-nuclear.pdf).

Appendix C

Neutron-skin uncertainties of Skyrme energy density functionals

This information was uploaded as an attachment (see Neutron-skin.pdf).

Appendix D

Landscape of Two-Proton Radioactivity

This information was uploaded as an attachment (see 2proton-radioactivity.pdf).

D.1 Erratum

This information was uploaded as an attachment (see 2proton-erratum.pdf).

Vita

Noah Watson Birge was born in Des Moines, Iowa and grew up in Dallas, Texas. In high school, he excelled in mathematics and science courses, but did not develop a serious interest in physics until his second year as an undergraduate at The University of Tennessee at Knoxville. At that time, he changed his major from a pre-medicine concentration to an academic physics and mathematics double major. In his last year as an undergraduate, he began working in Dr. Witek Nazarewicz's Nuclear Theory group and developed a particular interest in the group's work. Consequently, he remained at the University of Tennessee for his graduate career, continuing his work in Dr. Nazarewicz's research group.